AerospaceEurope Conference2021
WARSAW, POLAND | 23 -26 NOVEMBER 2021
CEAS Council of European Aerospace Societies

AEROELASTIC-TAILORING OF A WIND-TUNNEL MODEL FOR PASSIVE ALLEVIATION OF STATIC AND DYNAMIC LOADS

Nicolò Fabbiane[1], François-Xavier Irisarri[2], Johannes Dillinger[3] & Arnaud Lepage[1]

[1]DAAA, ONERA – Université Paris-Saclay, 29 av. de la Division Leclerc, 92322 Châtillon, France
[2]DMAS, ONERA – Université Paris-Saclay, 29 av. de la Division Leclerc, 92322 Châtillon, France
[3]DLR – Institute of Aeroelasticity, Bunsenstr. 10, 37073 Göttingen, Germany

Abstract

Composite materials allow to tailor the material elastic properties in the structures. In aeroeaslticity, this opens up the possibility to passively enhance the coupled aerostructural characteristics. In this work, the design of a composite wing is addressed with the aim to alleviate static and dynamic aeroelastic loads; these two objectives are quantified by the root-bending-moment in a high load-factor condition and the deformation amplitude of the wing under gust. A two-step approach of the optimal design of the structure is adopted. A Pareto front is computed via an aeroelastic model of the wing; the aerodynamic loads are modelled, depending on the load-case, either via the DLM or the RANS equations. The best-compromise design is chosen via a criterion based on the jig-shape and, finally, the stacking-sequences are computed via a specialised evolutionary algorithm.

Keywords: aeroelastic tailoring, passive load-alleviation, gust response, composite materials, bi-objective optimisation.

1. Introduction

Aeroelastic-tailoring can be defined as “the embodiment of directional stiffness into an aircraft structural design to control aeroelastic deformation, static or dynamic, in such a fashion as to affect the aerodynamic and structural performance of that aircraft in a beneficial way” [14]. The consolidation of composite material technologies spread even further the design capabilities in this direction. Several studies have been dedicated to this topic in the last decades [see 7, for an extended and exhaustive review], each one focusing on different aspects of the problem: optimisation to static loads [4], blending constraints [8, 1], and gust response [13], to cite some of the most recent developments.
This work aims to evaluate the potential of aeroelastic-tailoring by conceiving a composite wing to be tested by means of wind-tunnel experiments, as a part of a larger project that sees the collaboration of ONERA and DLR. The construction of two wind-tunnel demonstrators – one for each institution – is previewed with the general objective to passively alleviate gust-loads.
The design of the ONERA model is here presented. After a brief introduction to the wing-geometry, optimisation variables, and parameters (Section 2), the optimisation procedure and the sizing load-cases are discussed (Section 3). The optimal design-points are presented in the form of a Pareto-front and, between them, the final design is chosen (Section 4). Finally, the stacking-sequence is computed (Section 5), leading to manufacturing.

2. Geometry and structural parameters

The geometry is based on the Common Research Model [11]; the flight-shape used in the model-design is obtained by scaling the CRM geometry to a root-to-tip span equal to 550 mm, resulting in a root chord and reference surface of approximately 248 mm and 729 cm^2.
The structural configuration of the wing is given by two composite skins – upper and lower –, filled by a polymeric foam; the simplicity of this configuration has been chosen to ease the manufacturing

	$E_{(1)}$ (GPa)	$E_{(2)}$ (GPa)	$\nu_{(12)}$	G (GPa)	ρ kg/m^3	h_{ply} mm	ε_t mε	ε_c mε	ε_s mε
ply	31.3	5.34	0.29	1.90	1727	0.17	30	20	20
foam	0.095	–	0.30	0.014	80				

Table 1 – Materials' properties.

process, due to the small size of the model. The material of choice for the wing-skin is a glass-fiber/epoxy composite with a fiber volume-fraction equal to 0.39; a standard low-density polymeric foam is instead adopted for the filling, see Table 1. The uni-directional composite ply is considered as an orthotropic material with its first principal direction oriented as the fibers; the thickness of a single ply is 0.17 mm and it can withstand deformations in tension (ε_t), compression (ε_c), and shear (ε_s) up to 30 mε, 20 mε, and 20 mε respectively.
A finite-element (FE) model of the wing structure is created in NASTRAN [10] by discretising the composite-skins by quadrangular plate-elements and the internal foam by hexahedral volume-elements. A clamp boundary-condition is considered at the root section.

2.1 Design variables and parameters

Laminated composite plates are obtained by stacking different composite plies that, in the general framework, could have their own properties and thickness, as well as their own orientation. For this study, a single prototype ply is considered and the different stacks will only differ by the number and the orientation of the plies. The order in which the different plies are stacked is called *stacking-sequence*, that drives the mechanical behaviour of the laminate-plate. The latter can be locally expressed in the form of the constitutive law,

$$\begin{bmatrix} F \\ M \end{bmatrix} = \begin{bmatrix} A & B \\ B & D \end{bmatrix} \begin{bmatrix} \varepsilon \\ \kappa \end{bmatrix} \tag{1}$$

where F and M are the local in-plane and bending loads applied to the composite stack and ε and κ the local strains and curvatures of the plate [15]. The relation between load and deformation is given by the stiffness matrix. This can be divided in: (i) A that describes the *membrane* behavior, i.e. the direct link between F and ε; (ii) D that describes the *bending* behaviour, i.e. the direct link between M and κ; (iii) B that couples the two behaviours. All these matrices are a function of the stacking sequence; in particular, $B = 0$ when a symmetric stack is considered, as it is the case in this study.
The natural choice for the design variables would be the stacking-sequence itself. However, this poses some technical challenges, namely an optimisation with an undetermined number of variables and a non-smooth description of the functions of interest. A solution to this is given by the *lamination parameters* [9], i.e. a parameterisation of the stiffness matrix in Equation (1) that is based on the homogenisation of the composite stack. The local properties of the material are hence described by the relations,

$$\begin{aligned} A &= h \left(\Gamma_0 + \Gamma_1 \xi_1^A + \Gamma_2 \xi_2^A + \Gamma_3 \xi_3^A + \Gamma_4 \xi_4^A\right) \\ D &= \tfrac{h^3}{12} \left(\Gamma_0 + \Gamma_1 \xi_1^D + \Gamma_2 \xi_2^D + \Gamma_3 \xi_3^D + \Gamma_4 \xi_4^D\right) \end{aligned} \tag{2}$$

where $\xi^A_{1,2,3,4}$ and $\xi^D_{1,2,3,4}$ are the lamination parameters for the membrane stiffness-matrix A and bending stiffness-matrix D, h is the total thickness of the laminate plate, and Γ_i are the Tsai-Pagano material parameters of the composite ply [16].
The design variables are hence defined as the total thickness h and the 8 lamination parameters $\xi^A_{1,2,3,4}, \xi^D_{1,2,3,4}$; the homogenised properties of the laminated plate are considered uniform in each of the 10 design-zones in Figure 1, resulting in a total of $(1+8)\times 10 = 90$ design variables. To ensure that the solutions are representative of actual laminates, compatibility conditions have to be enforced between the membrane and the bending lamination parameters as additional constraints to the optimisation [3]. Lower and upper limits are enforced on the laminate thickness for manufacturing and geometrical reasons: the total thickness h is hence bounded between 1.70 mm (10 plies) and 3.74 mm (22 plies).

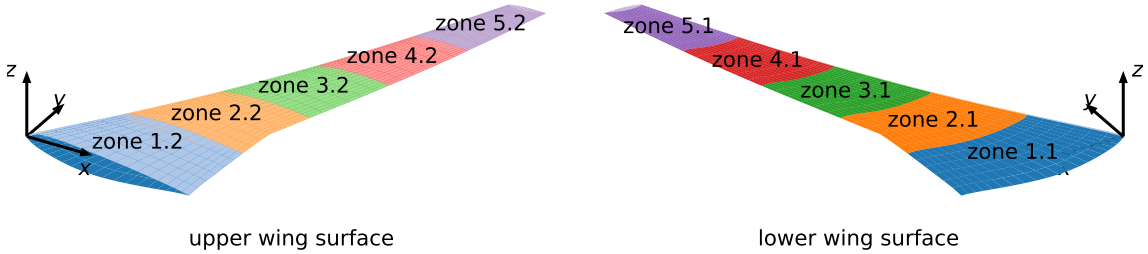

Figure 1 – Wing-geometry and regions for the composite-optimisation.

	cruise	**max-load**	**gusts**
type	static	static	equiv. static
method	RANS solver (rigid flight-shape)	DLM + FE model (aeroelastic trim)	DLM + FE model (aeroelastic response)
flight conditions	$M = 0.85,\ q = 31.95$ kPa, and $U = 276$ m/s		
	$c_L = 0.5$	$c_L = 1.0$	5 *worst* cases
	$Re \approx 4 \times 10^4$		$\Delta\alpha_g = 0.25°$
			$\{f_i\}_g = \{40, \ldots, 120\}$Hz
constraints	$-\varepsilon_c/3 < \varepsilon_{I,II} < \varepsilon_t/3$ and $\varepsilon_s^{max} < \varepsilon_s/3$		

Table 2 – Load-cases and constraints for the design procedure.

3. Design procedure

The goal of the design is to alleviate the static and dynamic loads on the wing, while respecting a prescribed flight-shape; this leads to specific choices on load-cases and optimisation strategy.

3.1 Load-cases and constraints

The considered load-cases span the typical sizing conditions for the aeronautic design (Table 2): a nominal cruise, a high load-factor condition and the response to gusts of variable time-scale. The asymptotic flow conditions are based on the ones expected in the wind-tunnel during the experiments; the Mach number M is chosen to match the design condition for the CRM model and the other quantities are computed based on the hypothesis of an isentropic flow. Similarly, harmonic gusts are considered due to limitations of the experimental gust-generation apparatus.

The loads representing the cruise condition are based on high-fidelity simulations via the in-house ONERA solver elsA [2]. The aerodynamic mean-flow is computed for the scaled CRM geometry of the wing, here taken as reference flight-shape and the angle-of-attack of the wing have been tuned to match the typical cruise condition of a lift coefficient C_L equal to 0.5. The retrieved pressure field is interpolated on the structural model – more precisely at the center of the plate-elements describing the composite skin – and, then, introduced as a pressure-load (f_{cruise}). The jig-shape of the wing is updated at each outer iteration of the design loop in order to ensure that the flight-shape is met under the precomputed cruise loads, see Algorithm 1.

The *max-load* case, instead, takes into account the aeroelastic behaviour of the wing in the loads computation. The doublets-lattice-method (DLM) is used as a model for the wing aerodynamic; a flat aerodynamic mesh is generated based on the form in plan of the wing and coupled to the structural FE model via the native tools available in MSC NASTRAN. Thanks to this aeroelastic model, the wing is trimmed, by acting on the angle of attack, to a lift coefficient equal to 1.0; this C_L value is chosen to represent a $2g$-maneuver.

The same aeroelastic model is also used in the evaluation of the gust loads. These will be taken into account in the optimisation procedure as equivalent-static-loads [12]; this method allows to take into account dynamic load-cases as static loads, based on the a dynamic simulation of the dynamic

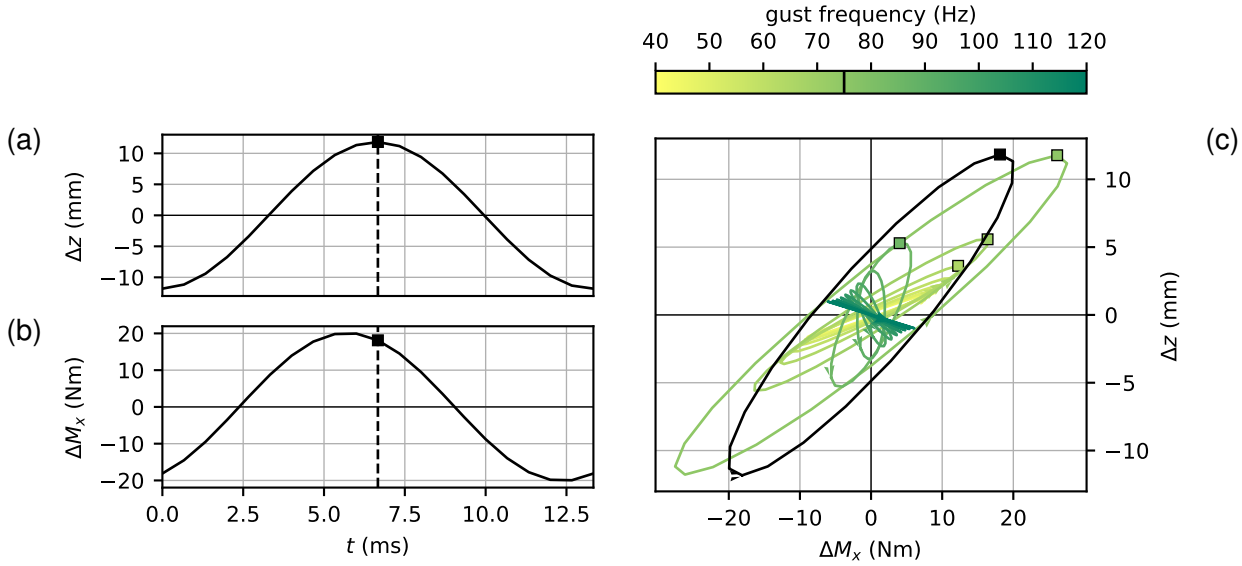

Figure 2 – Harmonic gust response and sizing conditions. (a-b) report the fluctuation of tip-displacement and root-bending-moment for a gust at 75 Hz and amplitude $\Delta\alpha = 0.25°$. The time of maximum tip-displacement is chosen as sizing-condition (black-square). The black line in (c) report the phase-diagram representation of the response in (a-b); the colored lines report the same response for different gust frequencies. The squares indicate the retained sizing-cases.

phenomenon of interest. In this work. harmonic gusts are considered: Figure 2(a-b) report the fluctuations of the tip-displacement and the root-bending-moment forced by an harmonic gust of frequency $f = 75$ Hz and amplitude $\Delta\alpha = 0.25°$. From this response, the time $\bar{t}$ that maximises the tip displacement is chosen as sizing state; the full displacement field $x'(\bar{t})$ is retrieved and the resulting equivalent-static-loads f are computed via the stiffness matrix of the complete structural model K as,

$$f = f_{cruise} + K x'(\bar{t}) \tag{3}$$

where the precomputed cruise-loads f_{cruise} are added to the fluctuation field. The forces thus calculated return, in a static simulation, a displacement field that will reproduce the dynamically computed gust response around the cruise condition. Only the gusts with the 5 largest tip-displacements are retained for the optimisation procedure, as reported in Figure 2(c), where it can be also noticed the change in phase-shift between tip-displacement and root-bending-moment when sliding in frequency. Strain constraints are enforced; principal and maximal-shear strains are extracted at top and bottom of each plate-element and limited by the values in Table 1, with a safety-factor 3.

3.2 Optimisation strategy

The optimisation loop is reported in Algorithm 1 for the general objective function $J(p;\pi)$, where p is the vector containing the design variables and π the one for the optimisation parameters. At each step of the outer loop, the equivalent static loads are recomputed for the retained gust-cases and fed to the MSC NASTRAN built-in optimiser; once the solution that optimises the general cost function J has been found, the jig-shape is updated via the new stiffness matrix. This loop is repeated N times; in the last M outer steps the thickness of the laminate-plates is fixed to an integer multiple of $2h_{ply}$ and only the lamination parameters are optimised. This improves, at least from a thickness point-of-view, the feasibility of the identified optimal-solution and it will facilitate the identification of the corresponding stacking-sequence.
The number of external steps N is set to 10, with $M = 3$ rounded-thickness iterations.

4. Pareto front

The choice of the cost function J drives the optimisation; since the aim is the alleviation of both static and dynamic aeroelastic loads on the wing, a bi-objective strategy is pursued. On the static

Algorithm 1: Design loop when minimising the generic cost function J

for $n \leftarrow 0$ **to** $N-1$ **do**

Collect the equivalent-static-loads $\{f_i\}_g$ *for the harmonic gust cases* $\{f_i\}_g$

forall $f_i \in \{f_i\}_g$ **do**

Solve the forced, aeroelastic problem

solve: $M\ddot{x}' + (K^{(n)} + K_a(f_g; M))x' = \Delta\alpha_g B_g \cos(f_g t/2\pi)$ [sol 146]

Compute the equivalent static loads for the time of maximal tip-displacement

return $f_i \leftarrow f_{cruise} + K^{(n)} x'(\bar{t})$ [sol 101]

if $n \leq N - M$ **then** $p := \{\{h, \xi^A_{1,2,3,4}, \xi^D_{1,2,3,4}\}_i\}$ $\pi := \{\Gamma_0, \Gamma_1, \Gamma_2, \Gamma_3, \Gamma_4\}$

else

Round the thickness to the closest integer multiple of $2h_{ply}$

forall $h \in \{h_i\}$ **do** $h \leftarrow \text{round}\left(h/(2h_{ply})\right) 2h_{ply}$

Re-define the design variables to lamination parameters only

$p := \{\{\xi^A_{1,2,3,4}, \xi^D_{1,2,3,4}\}_i\}$ $\pi := \{\{h\}_i, \Gamma_0, \Gamma_1, \Gamma_2, \Gamma_3, \Gamma_4\}$

Composite material optimisation

minimise $J(p; \pi)$ [sol 200]

p

loads and constraints: See Table 2 + compatibility conditions for $\xi_i^{(\cdot)}$

Update jig-shape

$x_{jig}^{(n+1)} \leftarrow x_{cruise} - K^{(n+1)^{-1}} f_{cruise}$ [sol 101]

When NASTRAN is used in a step, the solution type is reported in squared brackets.

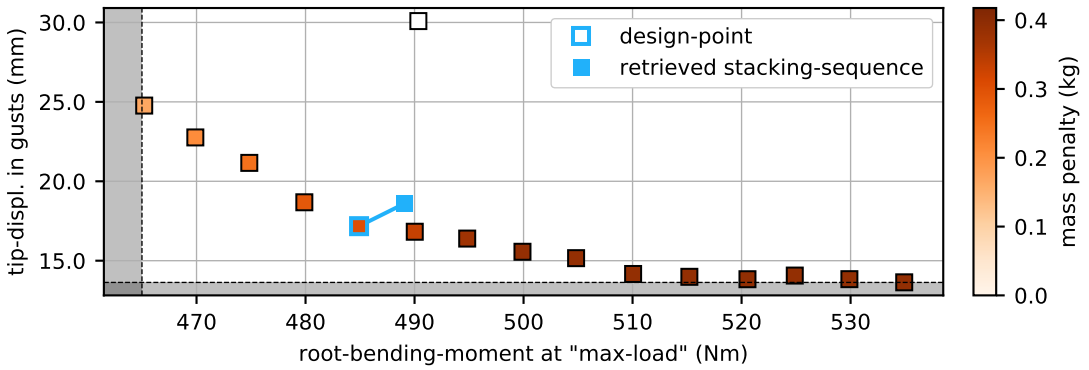

Figure 3 – Pareto front. The color-scale report the mass penalty with respect to the optimal-mass solution, here in white. The light-blue contoured point is the selected design-point, while the light-blue square reports the performance of the retrieved stacking-sequence (see Section 5 and Figure 7). The optimal limits for the two cost functions are reported by the shaded areas.

side, the objective is to minimise the root-bending-moment for the max-load case and, by this, to alleviate the structural loads when an off-cruise condition is encountered. On the dynamic side, an ensemble measurement of the response to the harmonic gusts is considered: this is quantified by the root-mean-squared of the tip-displacement on the retained gust-loads.

Figure 3 reports the Pareto front obtained for these two objective functions. As a first step, the optimal-mass design is computed and used as a reference point (white square). Starting from this solution, the boundaries for the two cost-functions of interest are calculated (vertical and horizontal dashed lines) and, finally, the points that trace the Pareto front. The color-scale indicates the distance in mass from the reference solution.

An ε-constrained method is used to identify these points [5]; this method consists in a series of

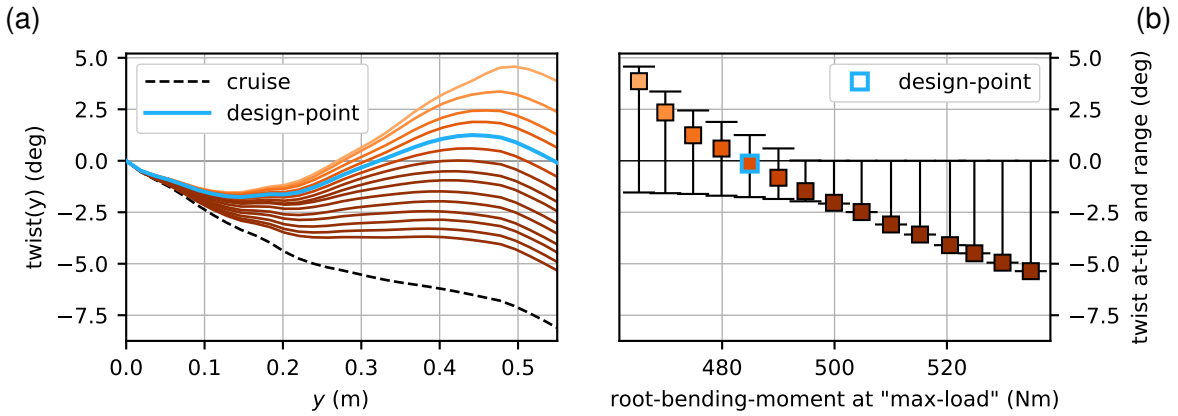

Figure 4 – Design-point criterion. The jig-shape twist is reported in (a) for each point of the Pareto-front in Figure 3. Squares and error-bars in (b) report the twist at the wing-tip and twist-range, as a function of the root-bending-moment.

consecutive optimisations for one of the cost functions – in this case, the gust response – while the other one – the root-bending-moment – is constrained to be lower than a certain value. In this manner, the Pareto front can be covered by computing the consecutive optimal points for the first (and free) objective, for increasing values of the second (and constrained) one. So that this strategy works, the two cost-functions are required to be antagonist to each other, condition that is verified for this choice of objective functions.
The jig-shape is computed as part of the optimisation procedure; Figure 4(a) shows how the twist-angle along the span coordinate y changes for the different points of the Pareto front. The distance between flight-shape and jig-shape is an indication of the overall flexibility of the wing, the larger the distance the more flexible the structure. Stiffer solutions are also heavier, and they are characterised by a larger root-bending-moment; as the flexibility increases, the wing becomes lighter, the root-bending-moment decreases at the cost of an increased gust-response.

4.1 Design-point

In a bi-objective optimisation, the definition of an unique design-point requires to arbitrarily pick a *best compromise* between the two objectives of the Pareto front; in this work, the jig-shape is considered as a criterion for this choice. Figure 4(b) resumes the information in Figure 4(a) and shows the twist at the wing-tip and the span-wise twist-range as a function of the root-bending-moment. The *flattest* jig-shape – i.e. the one with the most limited variation of twist angle – can be identified and chosen as the final design-point, light-blue square in Figures 3 and 4(b).
The value of the design variables at chosen design-point are visualised in Figure 5; the color-scale reports the local thickness of the laminate plate, while the polar-plots are a representation of the in-plane anisotropy of the constitutive law, i.e. how the stiffness of the base-ply is redistributed by the lamination parameters. This visualisation reports the engineering modulus,

$$E(\theta) = \frac{1}{T(\theta)^{-1} A^{-1} T(\theta)} \tag{4}$$

where θ is the polar angle, A is the membrane tensor, and $T(\theta)$ is the rotation operator for the deformation vector ε [4]; the red lines report the engineering modulus, while the blue ones a corresponding quantity computed for the flexion tensor D. The overall membrane-stiffness is oriented as the wing sweep; the misalignment occurs either for the flexion tensor or for marginal redistributions of the membrane-stiffness in the root region.
A further insight in the design process can be given by the constraints, since different wing regions are sized by different load-cases; Figure 6 shows, for each element, which load-case pushes the evaluated strains the closest to the constraint boundary. Two load cases rise from this analysis; the max-load that sizes the root-to-kink region and the 75 Hz gust that interests the rest of the wing. The first one only activates the constraints in a few elements in the kink region. The second one,

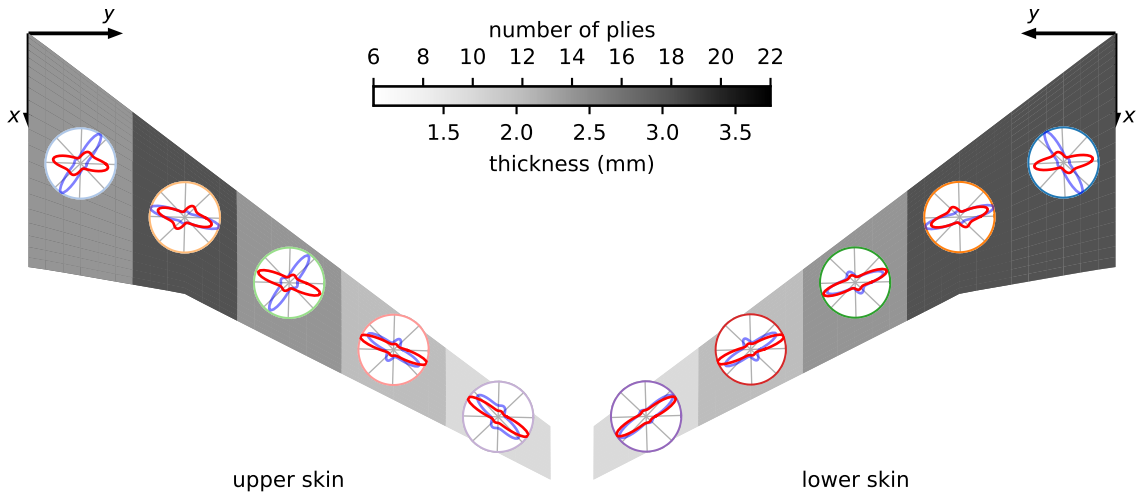

Figure 5 – Design point. The design variables – thickness and composite properties – are reported; the material properties are represented via the polar-plot of the engineering modulus, in red for the membrane-stiffness (A tensor) and in blue for the flexion one (D tensor).

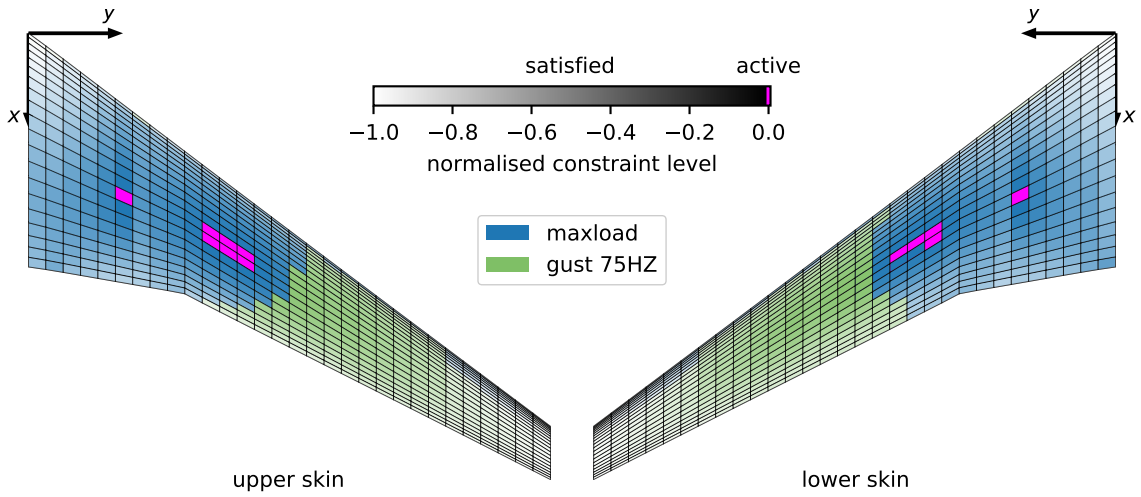

Figure 6 – Sizing load-cases. The color shows, for each element of the model, the load case that pushes the strains the closest to the failure envelope. The saturation indicates the proximity to the boundary; if the constraint is *active* – i.e. it is on the boundary within a normalised constraint value of 5×10^{-3} – the element is colored in magenta.

instead, affects the tip region, but with a constraint far from being activated; this is due to the imposed technological limit of a minimum of 10 plies that clearly oversizes the structure for strain constraint. It has to be noticed that this analysis returns only a view on the sizing by strain-constraint and it does not allow an insight of the role played by the load-cases in the objective-functions, of a more *global* nature.

5. Towards manufacturing

Up to this point, the constitutive law describing the laminate plates have been described via the lamination parameters, as introduced in Section 2.1 This description allows for an easier implementation of the optimisation algorithm but, on the other hand, it does not give the information needed to manufacture the laminate-plate; the stacking-sequence has thus to be recovered from the homogenised description by the lamination parameters. This task – called *inverse problem* – is a crucial point of the design procedure and, most importantly, its solution could be not unique (see for instance [17]). The inverse problem is here solved by a second optimisation via a specialised evolutionary algorithm

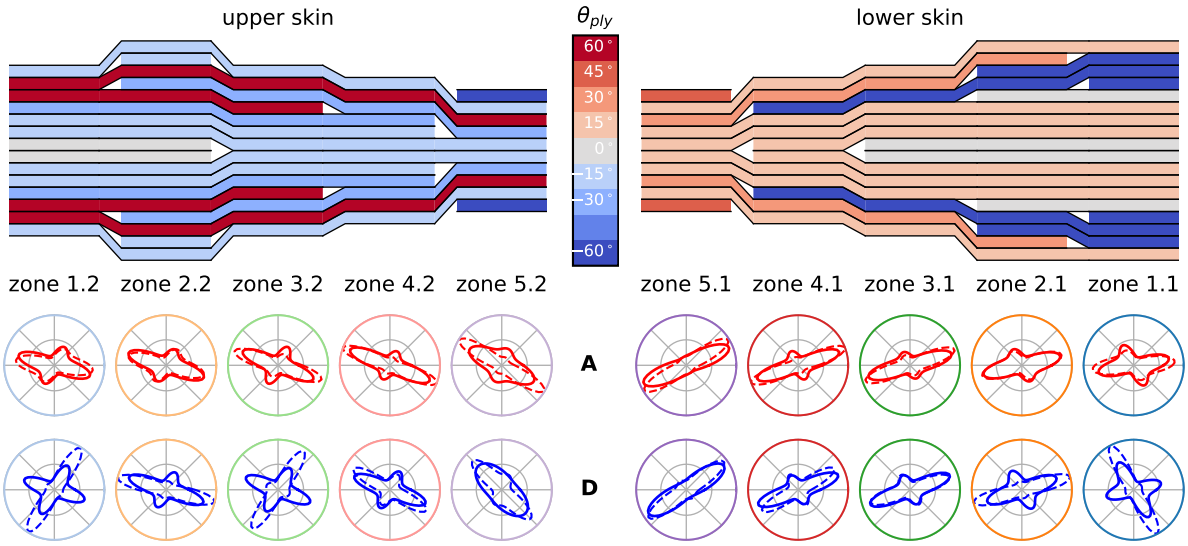

Figure 7 – Stacking-sequence for the upper (left) and the lower (right) skin. The bottom part of the figure shows, for the membrane and flexion tensors A and D, the deviation between the material properties prescribed by the continuous optimisation (dashed lines) and the properties for the retrieved stacking-sequence (solid lines).

based on the work by [6]; Figure 7 shows the identified stacking-sequence for the upper and lower skin; the gap between the design-point (dashed lines) and the retrieved stacking-sequence (solid lines) is minimised but it is still present. This is mainly due to the manufacturing constraints taken into account in the optimization: (i) ply angles are allowed to take value in the set $\{-60, -45, ..., 90\}$ and the ply thickness is fixed, which defines a discrete sampling of the design space; (ii) ply-continuity, or *blending*, is imposed between the regions in order to avoid strength-related issues. This significantly reduces the design space of the discrete optimization with respect to the design space of the continuous optimization. Indeed, all laminates are coupled due to the ply-continuity constraints, whereas they are assumed to be independent in the continuous optimization. Recent studies investigated the possibility of taking into account the *blending* problem by introducing additional constraints already at the stage of the lamination-parameter optimisation [e.g. 1].
Lastly, the performance registered by the identified stacking-sequence are reported on the Pareto front in Figure 3 by the red square; the root-bending-moment at max-load is higher as the gust response but it places in the vicinity of the design-point. All the strain constraints are satisfied and the wing results flutter-stable up to Mach 0.95 by a FEM-DLM analysis.

6. Conclusions

A composite wing is successfully designed to alleviate static and dynamic aeroelastic loads. The structure is built from two composite-skins each divided in 5 design-regions, where thickness and laminate properties – parameterised via the lamination-parameters formalism – are optimised.
A bi-objective optimisation is performed; based on the performance in a high-load condition and in gust. The optimisation process takes into account 7 load-cases; the nominal cruise, the high-load condition, and 5 load-cases representing the response to harmonic gusts with different frequencies. Among the multiple optimal-designs identified in the form of a Pareto front, the final design-point is chosen via a criterion on the jig-shape.
As the final step of a bi-step design-strategy, the stacking-sequences are retrieved for the identified design-point via a specialised evolutionary algorithm. The performance and constraints of the discrete, manufacturable solution are verified and compared with the continuous optimum. The here-presented design has been manufactured at DLR and wind-tunnel experiments took place at ONERA in the beginning 2021 to validate its performance against the here presented numerical simulations.

Acknowledgements

The authors would like to acknowledge Fabien Huvelin for the RANS simulations in cruise condition and Christophe Blondeau and Marco Tito Bordogna for the fruitful discussions and collaboration. The present work is part of the Common Research Project FIGURE – a collaboration between ONERA and DLR – and internal ONERA's research project CARACAL.

References

[1] M. T. Bordogna, P. Lancelot, D. Bettebghor, and R. De Breuker. Static and dynamic aeroelastic tailoring with composite blending and manoeuvre load alleviation. *Struct. Multidisc. Optim.*, 2020.

[2] L. Cambier, S. Heib, and S. Plot. The ONERA elsA CFD software: input from research and feedback from industry. *Mechanics & Industry*, 4(3):159–174, 2013.

[3] C. G. Diaconu and H. Sekine. Layup Optimization for Buckling of Laminated Composite Shells with Restricted Layer Angles. *AIAA Journal*, 42(10):2153–2163, 2004.

[4] J. K. S. Dillinger. *Static aeroelastic optimization of composite wings with variable stiffness laminates*. Phd thesis, TU Delft, The Netherlands, 2014.

[5] Y. V. Haimes, L. S. Lasdon, and D. A. Wismer. On a bicriterion formation of the problems of integrated system identification and system optimization. *IEEE Trans. Syst., Man, Cybern. Syst.*, SMC-1(3):296–297, 1971.

[6] F.-X. Irisarri, A. Lasseigne, F.-H. Leroy, and R. Le Riche. Optimal design of laminated composite structures with ply drops using stacking sequence tables. *Composite Structures*, 107:559–569, 2014.

[7] C. V. Jutte and B. K. Stanford. Aeroelastic tailoring of transport aircraft wings: State-of-the-art and potential enabling technologies. Technical Report NASA/TM-2014-218252, NASA, 2014.

[8] T. Macquart, N. Werter, and R. D. Breuker. Aeroelastic design of blended composite structures using lamination parameters. *J. Aicraft*, 54(2), 2016.

[9] M. Miki and Y. Sugiyama. Optimum design of laminated composite plates using lamination parameters. *AIAA J.*, 31(5):921, 1993.

[10] MSC Software. *MSC Nastran 2018 Design Sensitivity and Optimization User's Guide*, 2017.

[11] NASA CRM. Common Research Model. Website: page last modified on September 10, 2019. URL `https://commonresearchmodel.larc.nasa.gov/`.

[12] G.-J. Park. Technical overview of the equivalent static loads method for non-linear static response structural optimization. *Struct. Multidisc. Optim.*, 43:319–337, 2011.

[13] D. Rajpal, E. Gillebaart, and R. D. Breuker. Preliminary aeroelastic design of composite wings subjected to critical gust loads. *Aerosp. Sci. and Tech.*, 85:96–112, 2019.

[14] M. H. Shirk, T. J. Hertz, and T. A. Weisshaar. Aeroelastic tailoring - theory, practice, and promise. *Journal of Aircraft*, 23(1), 1986.

[15] S. W. Tsai and T. H. Hahn. *Introduction to composite materials*. Technomic Publishing Company, Lancaster, Pennsylvania, 1980.

[16] S. W. Tsai and N. J. Pagano. Invariant properties of composite materials. In S. W. Tsai, J. C. Halpin, and N. J. Pagano, editors, *Composite materials workshop, St. Louis, Missouri, 1967*, pages 233–253, Lancaster, Pennsylvania, 1968. Technomic Publishing Company.

[17] P. Vannucci and G. Verchery. Stiffness design of laminates using the polar method. *Intl. J. Solids and Struct.*, 38(50-51):9281–9294, 2001.